

Influence of plaque calcifications on coronary stent fracture: A numerical fatigue life analysis including cardiac wall movement

Stefano Morlacchi ^{a,b}, Giancarlo Pennati ^a, Lorenza Petrini ^c, Gabriele Dubini ^a,
Francesco Migliavacca ^{a,*}

^a Department of Chemistry, Materials and Chemical Engineering 'Giulio Natta', Politecnico di Milano, Milano, Italy

^b Department of Mechanical Engineering, University of Sheffield, Sheffield, UK

^c Department of Civil and Environmental Engineering, Politecnico di Milano, Milano, Italy

Article history:

Accepted 13 January 2014

1. Introduction

Coronary stent fracture (CSF) (Fig. 1A) has become an important issue in cardiovascular interventions. Preliminary reports based on follow-up angiographies quantified the incidence of CSF after drug-eluting stent implantation between 1% and 2% (Aoki et al., 2007; Shaikh et al., 2008). However, more recent studies, which were based either on autoptic analyses or on novel imaging techniques with improved spatial and temporal resolutions (Nakazawa et al., 2009; Lim et al., 2008), showed that CSF occurred in up to the 30% of the investigated cases. The type and severity of stent fracture play a fundamental role in the clinical consequences of CSF. In fact, recent clinical studies proved that the effects of CSF can be extremely variable among patients, ranging from asymptomatic cases to

increased rate of target lesion revascularization, to stent thrombosis or even to sudden death (Kuramitsu et al., 2012; Adlakhia et al., 2010). Consensus on routine follow-up and diagnostic methods to detect and to treat CSF has not been reached yet. In this context, CSF still remains an unresolved clinical problem.

From a mechanical point of view, failure of metallic structures like stents can be classified according to two categories: i) rupture due to static forces when these cause a stress higher than the ultimate material limit (i.e. static rupture) or ii) rupture due to cyclic loadings which are lower than the ultimate material limit (i.e. fatigue rupture). In particular, coronary stents have to operate within an environment which is extremely challenging. After being implanted and highly deformed through balloon inflation, stents undergo cyclic loading caused by both the pulsatile blood pressure and the cardiac wall movement occurring during each heartbeat. Accordingly, anatomical studies proved that coronary arteries undergo important curvature changes throughout the cardiac cycle (Liao et al., 2002). Experimental and in vivo studies showed that several factors may be identified as independently responsible for CSF. Among these, the presence of overlapping

* Correspondence to: Laboratory of Biological Structure Mechanics, Department of Chemistry, Materials and Chemical Engineering 'Giulio Natta', Politecnico di Milano, Piazza Leonardo da Vinci 32, 20133 Milano, Italy. Tel.: +39 02 2399 4316; fax: +30 02 2399 4286.

E-mail address: francesco.migliavacca@polimi.it (F. Migliavacca).

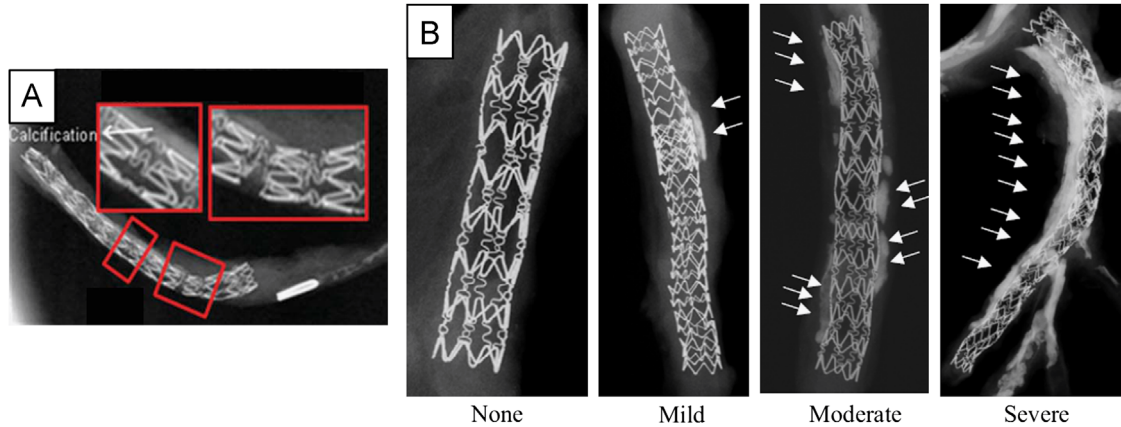


Fig. 1. (A) Example of coronary stent fractures on a Cypher vein graft stent in correspondence of a heavily calcified plaque. In the right inset is clearly visible how the stents split in two distinct parts. Image modified with permission from [Halwani et al. \(2012\)](#). (B) Different plaque calcifications in coronary arteries: the rightmost image shows a highly asymmetric calcified plaque. Arrows identify the location of mild, moderate or severe plaque calcifications. Image modified with permission from [Nakazawa et al. \(2009\)](#).

stents, plaque calcifications, high curvature of the vessel, length and design of the stent seem to play a role in CSF ([Nakazawa et al., 2009](#); [Halwani et al., 2012](#); [Aoki et al., 2007](#); [Shaikh et al., 2008](#)). In particular, plaque calcifications are currently considered as an active disease process similar to embryonic bone formation ([Hjortnaes et al., 2013](#)). Their initiating mechanisms are not fully understood yet, but they appear as a consequence of tightly regulated processes culminating in organized extra-cellular matrix deposition by osteoblast-like cells ([Johnson et al., 2006](#)). Eventually, the calcification process results in highly stiff bone-like structures, locally increase the heterogeneity of atherosclerotic plaques and their radial stiffness.

Computational models have been widely used for their ability to replicate the biomechanical response of medical devices under physiological conditions. Also, regulatory bodies have begun to consider computational modelling as a valid tool to evaluate intravascular stents through both pure stress/strain analyses and fatigue analyses ([FDA, 2010](#)). For this purpose, both static structural numerical models ([Martin and Boyle, 2011](#); [Morlacchi and Migliavacca, 2013](#)) and fatigue life studies ([Marrey et al., 2006](#); [Hsiao et al., 2012](#); [Schievano et al., 2010](#); [Li et al., 2010](#)) have been developed to provide new insights and, eventually improve both the clinical procedures and the stent design.

In this study, structural finite element models were implemented to simulate the stent expansion in a simplified model of epicardial atherosclerotic coronary artery and to investigate the effects of cyclic blood pressure and cardiac wall movement on the fatigue resistance of the stent. Two different cases were compared to quantify the response due to the presence of a localised calcification in the atherosclerotic plaques. The aim of this work was to provide a mechanical explanation of the increased risks of stent fracture when associated with the presence of plaque calcifications ([Fig. 1B](#)) ([Halwani et al., 2012](#)). Furthermore, since the current state-of-the-art mostly focuses on the effects generated by the blood pressure, the effects of either cardiac wall movement or blood pressure were explored to investigate their relative importance during fatigue analysis of coronary stents.

2. Material and methods

2.1. Finite element model of stent expansion

A finite element model of a simplified epicardial atherosclerotic coronary artery ([Fig. 2A](#)) was created using Rhinoceros 4.0 Evaluation

CAD software (McNeel and Associates, Indianapolis, IN, USA). The model of the coronary artery was embedded into the myocardium and characterized by a curvature radius of 20 mm ([Ding and Friedman, 2000](#)) and a total length of 31 mm. Lumen radius and arterial wall thickness were equal to 1.35 mm and 0.9 mm, respectively. The artery was surrounded by the cardiac wall for half of its circumference; the wall was assumed to be 7 mm thick, which is within the physiological range of adult human left ventricular walls ([Grossman et al., 1975](#)). The geometry was discretized with a total of 245,856 linear reduced integration hexahedral elements. In particular, 146,016 and 99,840 elements were used for the cardiac wall and the artery, respectively. A grid sensitivity analysis was performed to guarantee the independence of the solution from the spatial discretization. The material of the arterial wall was described as an incompressible isotropic and homogeneous material fitting the experimental data in the circumferential direction as obtained by [Holzapfel et al. \(2005\)](#) for the *tunica media*. In particular, the following reduced polynomial strain energy density function of the sixth order was implemented:

$$U = C_{10}(\bar{I}_1 - 3) + C_{20}(\bar{I}_1 - 3)^2 + C_{30}(\bar{I}_1 - 3)^3 + C_{40}(\bar{I}_1 - 3)^4 + C_{50}(\bar{I}_1 - 3)^5 + C_{60}(\bar{I}_1 - 3)^6$$

where C_{10} – C_{60} are the material parameters ([Table 1](#)) and \bar{I}_1 is the first deviatoric strain invariant. Experimental data were modified removing the first portion of the stress–strain curve up to 0.15 of strain. This assumption can be justified by the fact that the model of the artery was designed in a pressurized condition (radius=1.35 mm, diastolic blood pressure) while experimental tests were performed on fully unloaded tissues. The presence of the cardiac wall in the model is a convenient way to simulate the heart movement and transfer its cyclic kinematic displacements to the stented region, avoiding the presence of concentrated external boundary conditions close to the region of interest. An elastic material model was adopted for the cardiac wall with Young modulus and Poisson ratio equal to 20 MPa and 0.3, respectively. Simulations with Young moduli ranging between 2 and 40 MPa were also carried out to investigate the sensitivity of the model to this modelling assumption.

An asymmetric atherosclerotic plaque ([Fig. 2B](#)) was included in the model, taking into account the typical cross-sectional plaque distribution which is larger at the myocardial side of coronary arteries ([Iwami et al., 1998](#)). The maximum grade of stenosis value was equal to 60% of the arterial lumen and localised at the central section of the model. Two different models of atherosclerotic plaques were used, differing in the presence of a localised calcification within a homogeneous

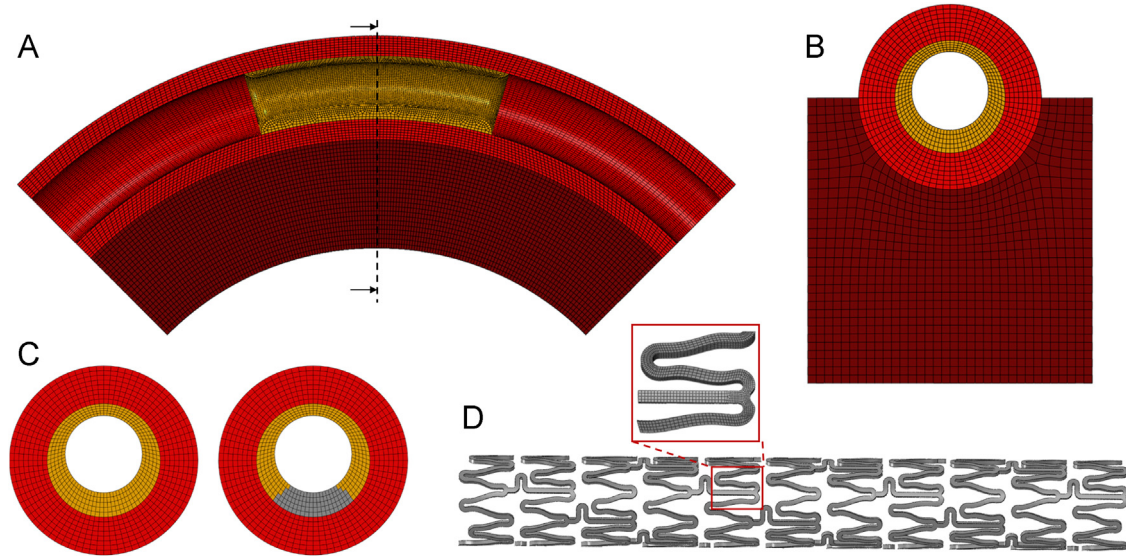


Fig. 2. (A) and (B) Model of the epicardial atherosclerotic coronary artery surrounded by the cardiac wall in its lower half. (C) Cross-sections of the vessels for the non-calcified and calcified (the calcification is in grey) models. The plaques show their asymmetric configuration with increased thickness close to the myocardium. (D) Stent model with an enlarged view of its mesh, which presents a finer discretization both in the area of connexion between links and struts and in the curves.

Table 1

Coefficients of the strain energy density function for the arterial wall and cellular plaque models. Experimental data from [Holzapfel et al. \(2005\)](#) and [Loree et al. \(1994\)](#) were used for the material model implementation.

	C_{10} [MPa]	C_{20} [MPa]	C_{30} [MPa]	C_{40} [MPa]	C_{50} [MPa]	C_{60} [MPa]
Arterial wall	2.689E-01	6.257E-01	-2.0913	21.953	-66.8425	74.9243
Cellular Plaque	2.38E-03	1.89E-01	-3.88E-01	3.73	-2.54	5.73E-01

matrix of cellular plaque (Fig. 2C). The total volume of the calcification was equal to 1.73 mm^3 . Discretization of the plaque resulted in a total of 42,560 linear reduced integration hexahedral elements. Sliding between plaque and artery was prevented by merging the nodes of the two parts. The hyperelastic behaviour of atherosclerotic plaque was modelled using the same strain energy density function used for the arterial wall and tuning the material parameters (Table 1) to fit the experimental data obtained by [Loree et al. \(1994\)](#) for cellular plaques. The inclusion of the calcification was simulated by providing a set of elements in the central part of the plaque with a stiffer elastic behaviour (i.e. Young modulus and Poisson ratio equal to 300 MPa and 0.3, respectively). Few experimental data are available on mechanical properties of large calcifications in atherosclerotic plaques. Those proposed by [Ebenstein et al. \(2009\)](#) showed that the stiffness of calcifications have a large variability ranging from 100 MPa to 10 GPa, thus contributing to increase the heterogeneous character of atherosclerotic plaques.

A model of a coronary stent was created by replicating the commercial stent Xience Prime (Abbott Lab., USA) (Fig. 2D). Its length, external diameter in the undeformed configuration and strut thickness were 13.02 mm, 1.76 mm and $80 \mu\text{m}$, respectively. The device was discretized with a total of 211,468 hexahedral elements and its mechanical properties were modelled by means of a Von Mises–Hill plasticity model with isotropic hardening, characterized by the following properties describing the behaviour of a typical Cobalt–Chromium alloy: 233 GPa, 0.35, 414 MPa, 930 MPa and 44.5% in terms of Young modulus, Poisson coefficient, yield stress, ultimate stress and deformation at break, respectively ([Poncin and Proft, 2003](#)).

A 3 mm diameter balloon for angioplasty was modelled and used to simulate the procedure of stent expansion in the coronary

artery. A total of 29,088 linear quadrilateral membrane elements were used to discretize the geometry. An isotropic elastic model was used to provide the balloon with semi-compliant mechanical behaviour. Elastic modulus and Poisson ratio were equal to 1455 MPa and 0.3, respectively ([Gervaso et al., 2008](#)).

Finite element analyses were run with the commercial software ABAQUS/Explicit (Dassault Systemes, Simulia Corp., RI, USA) to simulate the stent expansion as a quasi-static process. More details on this method are described in [Gastaldi et al. \(2010\)](#). Due to the curved shape of the artery, the stent underwent a preliminary simulation of crimping (reduction of diameter) and advancing (bending) in the correct position. In this way, the history of stent stress modifications before the deployment was accounted for ([Morlacchi et al., 2013](#)). The angioplasty balloon was then positioned inside the bent stent and inflated at 15 atm to simulate the stent implantation in both the models, with calcified and non-calcified plaques, respectively (Fig. 3). Elastic recoil was then allowed by deflating the angioplasty balloon.

2.2. Cyclic boundary conditions

After deployment in the coronary vasculature, stents undergo pulsatile loading conditions that arise from two different phenomena: oscillation of the internal blood pressure and cardiac wall movement. These phenomena were modelled by applying the loading and displacement boundary conditions illustrated in Fig. 4. In particular, the internal blood pressure oscillated between 80 and 120 mm Hg from diastole to systole and was applied to the internal surfaces of the artery, plaque and stent. In addition, a 4 mm radial displacement was applied to the nodes of the internal

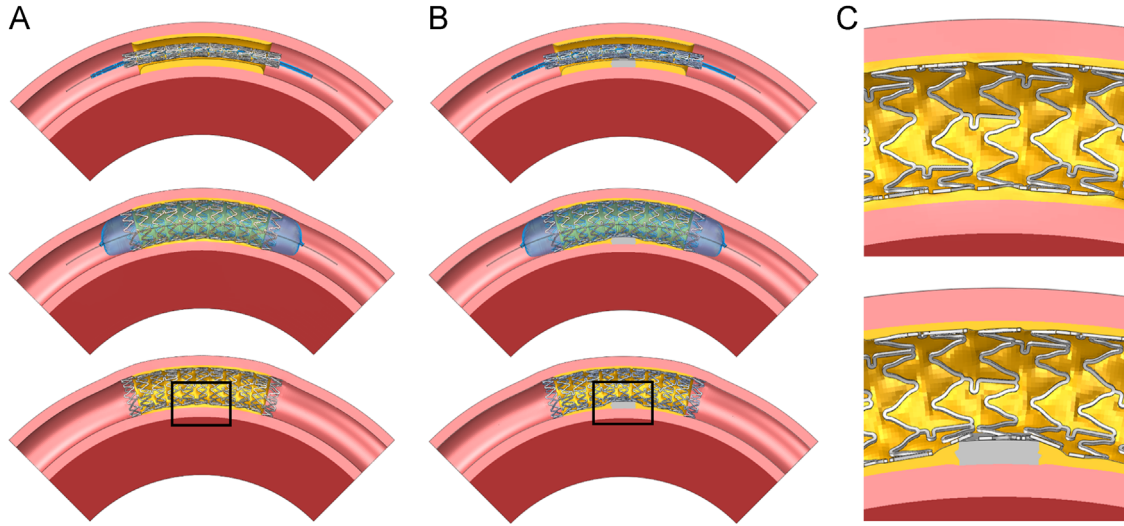


Fig. 3. After crimping and advancement in the central position of the artery, the stent is expanded by an angioplasty balloon in the curved atherosclerotic artery without (A) and with (B) localised calcification. (C) Magnification views in the central part of the models. The presence of the calcification does not allow the complete expansion of the device and generates higher deformations in the stent.

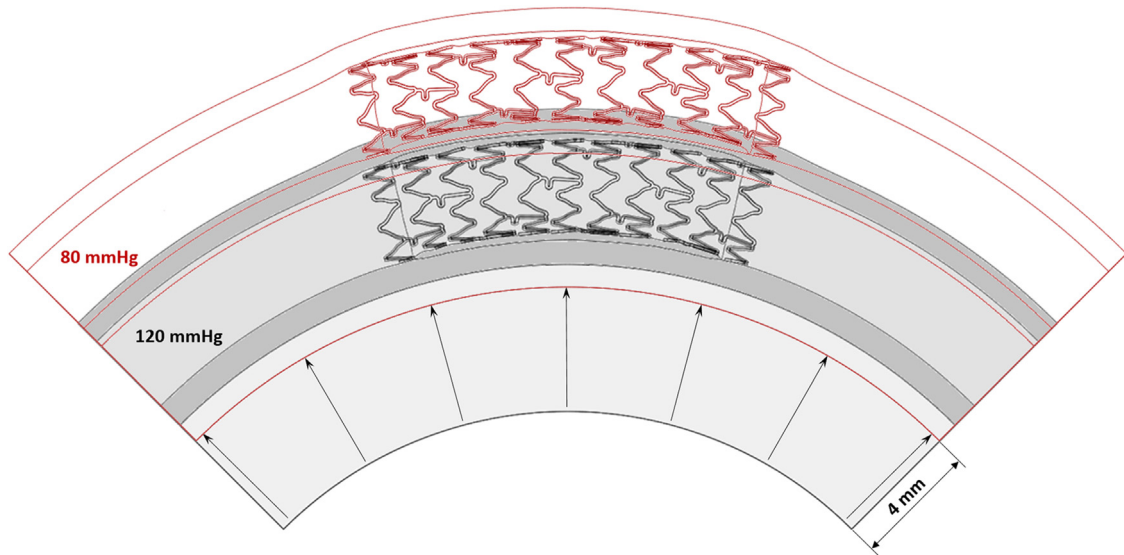


Fig. 4. Loads and displacement conditions applied to the model to simulate the cyclic loadings during the cardiac cycle. Systolic and diastolic configurations are illustrated in black and red, respectively (For interpretation of the references to colour in this figure legend, the reader is referred to the web version of this article).

cardiac surface to simulate the cardiac wall expansion. This condition contributed to a modification of the mean curvature of the artery from 0.5 cm^{-1} during systole to 0.4116 cm^{-1} during diastole (Prosi et al., 2004). Circumferential and axial displacements were fully constrained at inlet and outlet arterial surfaces. Diastolic heart filling and systolic contraction steps were simulated for three cardiac cycles (Fig. 5).

2.3. Fatigue life analysis

Stress values obtained after the second cycle were equal to those obtained after the third cycle; hence, a Goodman life analysis was performed using the oscillating multi-axial stress state obtained during the second cardiac cycle.

In particular, after collecting the values of the principal stresses (σ_1 , σ_2 and σ_3) at each node, effective mean and alternate stresses

were calculated using the following equations:

$$\sigma_m = \frac{1}{\sqrt{2}} \sqrt{(\sigma_{1m} - \sigma_{2m})^2 + (\sigma_{2m} - \sigma_{3m})^2 + (\sigma_{3m} - \sigma_{1m})^2}$$

$$\sigma_a = \frac{1}{\sqrt{2}} \sqrt{(\sigma_{1a} - \sigma_{2a})^2 + (\sigma_{2a} - \sigma_{3a})^2 + (\sigma_{3a} - \sigma_{1a})^2}$$

where σ_{1m} , σ_{2m} and σ_{3m} are the principal mean stresses, while σ_{1a} , σ_{2a} , and σ_{3a} are the principal stress amplitudes. These values were used to build Goodman diagrams that are commonly used to quantify the combined effect of mean and alternating stresses on the fatigue life of a material. Points falling below the limit line of the material should not fail for fatigue rupture; on the other hand, the points over the limit line are more likely to rupture. Due to lack of exact information on the mechanical behaviour of the material used to fabricate the stent, limit values for a generic

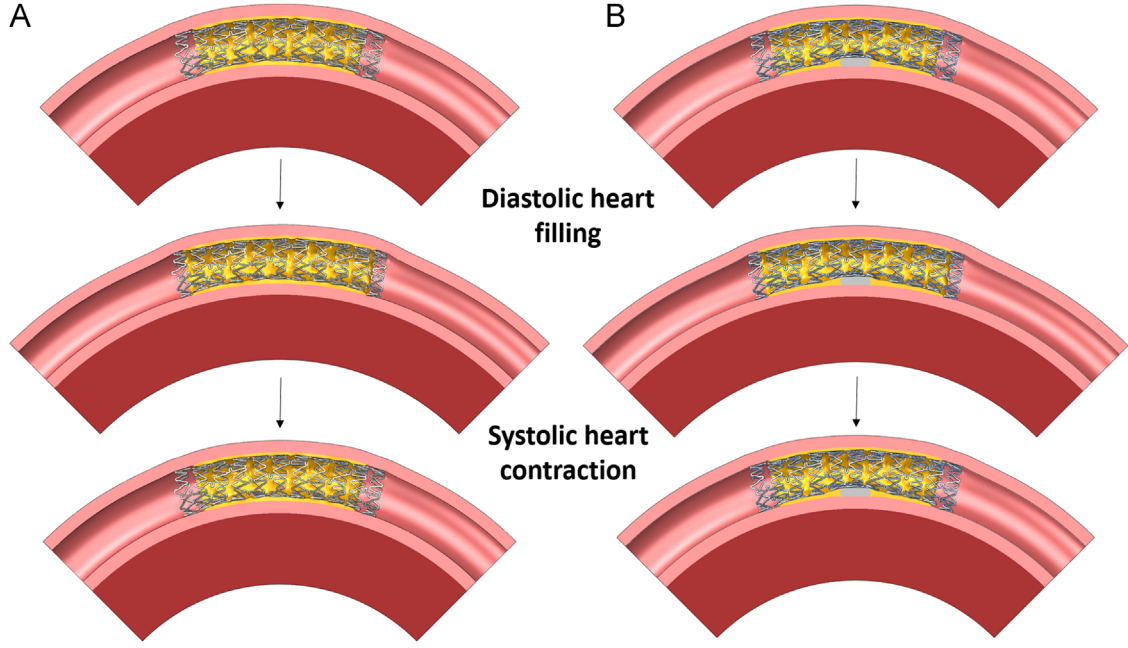


Fig. 5. Geometrical configurations of the myocardium, artery and stent during the simulation of the cardiac cycle in case of atherosclerotic artery without (A) and with (B) localised calcification.

medical Cobalt–Chromium alloy were used to draw the stent material fatigue limit on the Goodman diagram. In particular, the endurance limit for zero mean stress was assumed equal to 483 MPa (Hsiao et al., 2013) while ultimate stress was equal to 930 MPa (Poncin and Proft, 2003). Furthermore, the inverse of the Fatigue Safety Factor (FSF) was calculated to quantitatively express the risk of fracture. Values greater than unity correspond to the nodes above the material limit line of the Goodman diagram. The following definition of FSF was used:

$$\frac{1}{FSF} = \frac{\sigma_m}{S_{ult}} + \frac{\sigma_a}{S_a}$$

where σ_m is the effective mean stress, σ_a is the effective alternate stress, S_{ult} is the ultimate stress and S_a is the endurance limit for zero mean stress. In order to quantitatively compare two Goodman diagrams, the volume of material at risk was calculated for each ring of the stent and normalized with the initial volume of the ring using the following formula:

$$\frac{V_{RISK}}{V_0} = \frac{\sum_1^N V_{RISK_i} (n_i/8)}{V_0}$$

where V_{RISK_i} is the volume of the i -th elements with at least one node falling on the critical region of the Goodman diagram for fatigue fracture, n_i is the number of nodes of the i -th element over the Goodman line and V_0 is the volume of the whole ring.

Two different fatigue analyses are presented in this work. The first one investigates the influence of plaque calcifications on the fatigue failure risk by comparing the Goodman diagrams obtained in the case of homogeneous atherosclerotic cellular plaque and in the case of cellular plaque with localised calcification. The latter investigates the independent effects of blood pressure oscillations and cardiac wall displacement on the stent fatigue behaviour. In such a way, the relative contribution of each phenomena may be assessed to better understand the importance of their modelling during the fatigue analysis of coronary stents.

3. Results and discussion

3.1. Influence of plaque calcification: stress/strain analysis

Results of the simulations in terms of geometric deformations (Fig. 6) at the end of the stent expansion showed how the presence of a localised calcification generated a greater resistance to vessel opening inducing a stent protrusion towards the centre of the lumen. In addition, slightly higher stresses were observed in the stent struts close to the calcified region. Quantitatively, the maximum Von Mises stress in the case of fully cellular plaque was 798 MPa. This value increased up to 819 MPa in the presence of a plaque calcification. Accordingly, plaque calcification proved to be a relevant mechanical occurrence, underlying the importance of a model including the plaque heterogeneities which might increase the risk of static failure of metallic stents.

3.2. Influence of plaque calcification: fatigue life analysis

The effects of cyclic loading on the stent fatigue resistance were assessed in terms of Goodman diagrams (Fig. 7) and Fatigue Safety Factor (Fig. 8) for both the plaque models with and without localised calcification. In a Goodman diagram, points are defined by the mean and alternate stress values occurring during a loading cycle. If the point is close or exceeds the material limit, a higher risk of fatigue fracture arises at the point location.

A comparative analysis of panels in Fig. 7 indicates that the presence of a localised plaque calcification increases the risk of fatigue fracture. This finding is in agreement with experiments reported in literature (e.g. Halwani et al. (2012)). This result is confirmed, when considering only the struts close to the calcification.

Fig. 8A shows the elements with at least one node characterized by $1/FSF$ values greater than 1 (i.e. above the material limit line). Through a finite element analysis, it is possible to localise such points in the curved hinges of the struts. In addition, their presence increases in the central part of the stent, which directly interacts with the calcified region. This observation is quantified in the plot shown in Fig. 8B where the volume of the material at

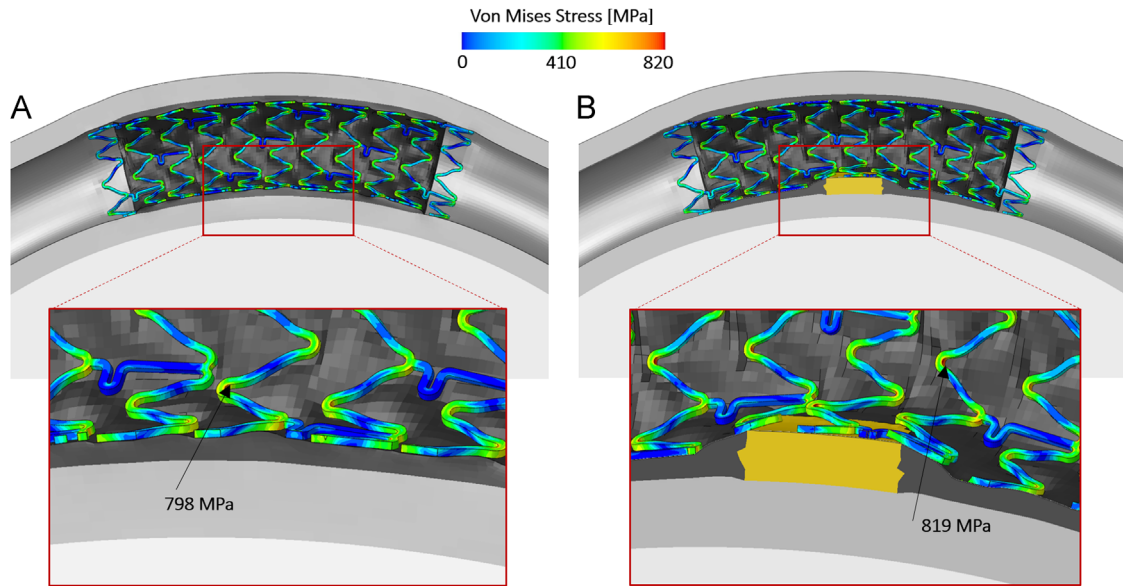


Fig. 6. Contour maps of the Von Mises stresses after stent deployment in the atherosclerotic arteries without (A) and with (B) calcification. The presence of a localised calcification induces higher and different stress patterns in the stent. Black arrows point out the maximum values obtained.

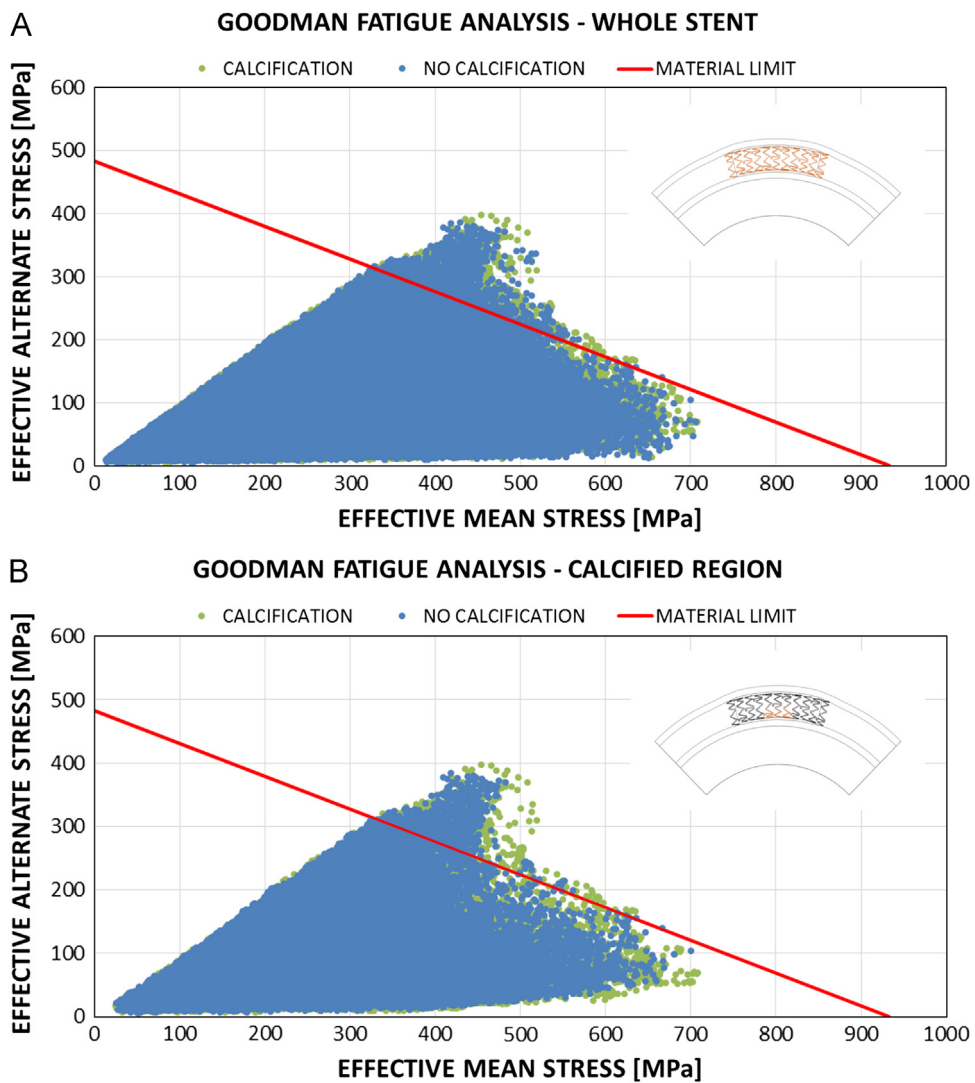


Fig. 7. Goodman diagrams for the atherosclerotic artery without (blue) and with (green) localised calcification. Values of the effective mean and alternate stresses are calculated at each node of the whole stent (A) or only in the struts close to the calcified region (B). The red line refers to the limit of the stent material: points above the line are considered at high risk of fatigue failure (For interpretation of the references to colour in this figure legend, the reader is referred to the web version of this article).

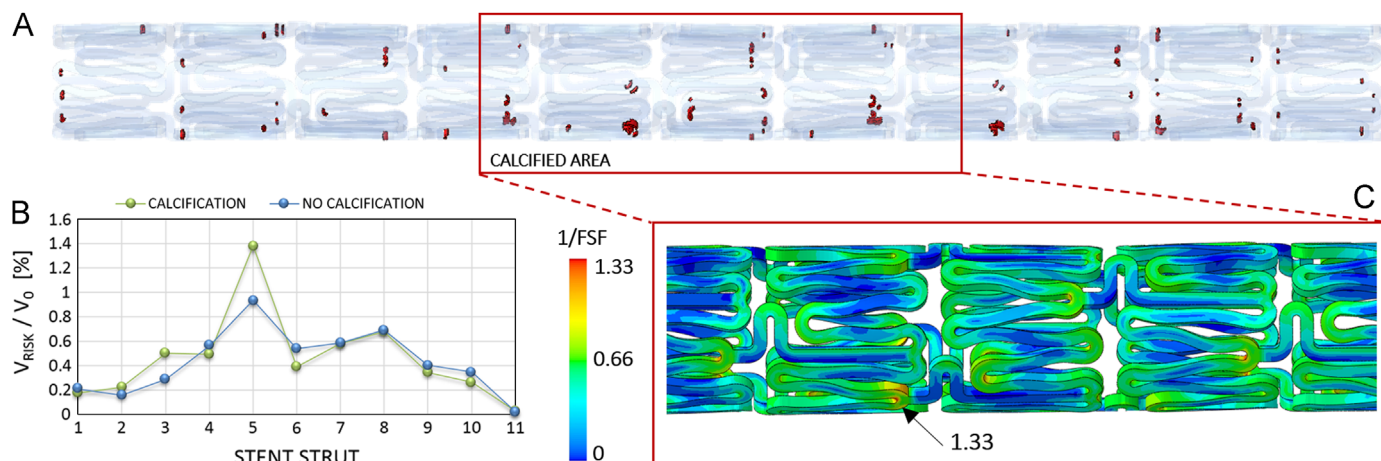


Fig. 8. Analysis of the Fatigue Safety Factor (*FSF*) in the case of localised calcified plaque. (A) Visualization of the elements whose nodes have the inverse of the *FSF* greater than 1 and are at higher risk of rupture. (B) Plot presenting the ratio between the volume at risk of fracture and the total volume calculated per each stent ring for both the calcified (green line) and non-calified case (blue line). The struts close to the calcified region (5, 7) are characterized by a peak of the volume of material at risk. (C) Contour map of $1/FSF$. The black arrow shows the maximum value obtained in the calcified region (For interpretation of the references to colour in this figure legend, the reader is referred to the web version of this article).

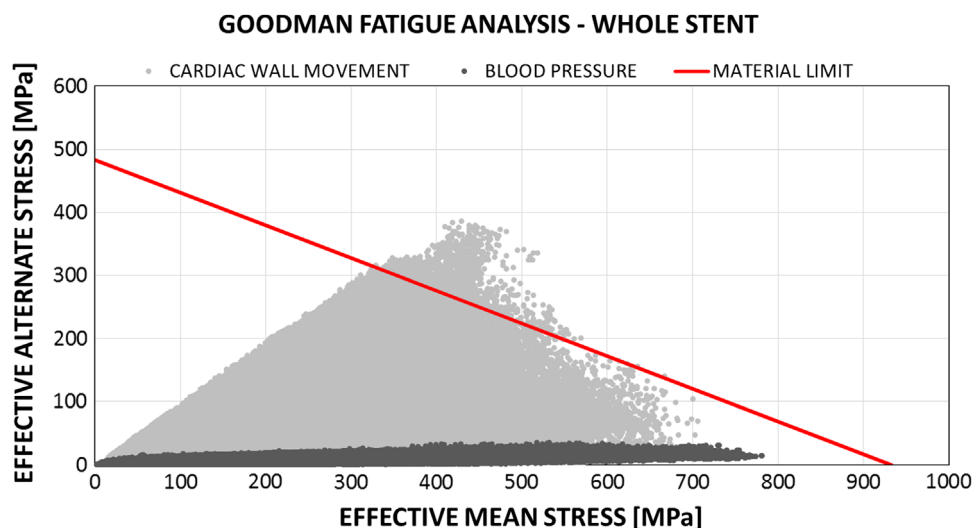


Fig. 9. Goodman fatigue analysis. Independent effects of cardiac wall movement (light grey) vs. blood pressure (dark grey).

higher risk of fracture is calculated for each ring of the stent in both the scenarios (i.e. with and without calcification) and normalized over the initial volume of the stent strut. Hence, the fifth ring was found to be the most critical area in both cases, with a 1.40% of volume at risk of fracture in case of plaque calcification. This value dropped to 0.96% in the case of homogeneous cellular plaque. Fig. 8C shows the contour map of the inverse of the *FSF* displayed for the case of calcified plaque. The highest values were concentrated near to the curved struts of the stent (i.e. maximum value 1.33). In the case of plaque without calcification, the maximum value was 1.22.

3.3. Effect of cardiac wall movement and blood pressure on the stent

In Fig. 9, the independent effect of cardiac wall displacement and pulsatile blood pressure is compared through a Goodman diagram calculated for the whole stent in case of cellular plaque. Results show that the cardiac wall movement has a greater effect on the risk of fracture in comparison with the blood pressure. This finding highlights the importance of including model of the

myocardium for the analysis of fatigue risk of coronary stents. From a mechanical point of view, a pressure variation of 40 mm Hg is unable to affect the stress values in the metallic structures, which are characterized by a very stiff behaviour. In this scenario, the maximum alternate values obtained in the stent were around 35 MPa. These values are comparable to those obtained in previous studies (Marrey et al., 2006; Argente dos Santos et al., 2012; Hsiao et al., 2012, 2013). On the other hand, the cardiac wall displacement provoked alternating stress values up to 390 MPa. Importantly, in both cases no additional plastic deformations occurred in the stent during the cyclic loadings, demonstrating that periodic loadings only work within the elastic range of the material.

3.4. Model limitations

This study presents a novel modelling framework to assess the risk of fracture of stents implanted in coronary arteries. Some modelling assumptions were made and are hereafter listed. Accordingly, specific statements on particular stent design or

clinical scenarios cannot be made and the proposed results should only be used for comparative purposes.

The geometries used are highly idealized and may only be useful to provide general guidelines. In our model, only one curvature and one type of calcific lesion were investigated, limiting our conclusions to this specific case. In order to generalize our results, a sensitivity analysis on arterial curvature or dimension of calcifications should be performed. The presence of highly and diffused asymmetric calcified segments might produce effects different from those reported here. Indeed the 'indentation' effect generated by a 'localised' plaque might produce more dangerous consequences than more diffuse calcified segments. Moreover, in order to adopt such methods in the clinical field, patient-specific image-based geometries should be included to better characterize the geometrical features of the coronary arteries in terms of vessel curvature, dimensions and plaque composition (Gijzen et al., 2008; Morlacchi et al., 2013). Currently, very accurate strategies of image-based 3D reconstruction of coronary arteries are not available yet. In the future, imaging modalities such as Optical Coherence Tomography (OCT), which are able to identify the different components of atherosclerotic plaques, might be exploited for this purpose (Bouma et al., 2003; Celi et al., 2013).

Material modelling of arterial tissues was simplified by neglecting the arterial stratifications and their anisotropic behaviour. Heart contraction was simulated through displacement boundary conditions, while the mechanical behaviour (i.e. stiffness) of the cardiac wall did not change during diastole and systole. However, accurate mechanical representation of the myocardial wall was not a primary goal of this work, as the wall model was used to provide kinematic boundary conditions to the stented vessel. The myocardium is modelled as a stiff material and this assumption might influence the deformation of the stent to some extent. For this purpose, a sensitivity analysis of this choice was performed by varying the myocardium Young modulus between 2 MPa and 40 MPa. Results in terms of stress state are slightly influenced both in the stent and in the vessel. A softer myocardium increases the effect of plaque calcification in inducing stent fracture and marginally reduces the stresses in the arterial wall caused by blood pressure. However, we believe that the main results of this study are not affected by this simplification.

Plaque modelling was also simplified mainly because of the lack of experimental data. Homogeneous and isotropic behaviour were assumed to describe the cellular plaque and a linear elastic model was used for the calcification. No damage model of the tissue was included in the simulations.

Finally, only one stent was investigated while different design features might result in a range of abilities to resist fatigue fracture.

However, all these simplifications can be accepted as the main aim of the study was a comparative analysis of the mechanical behaviour of a generic coronary stent under different working conditions.

4. Conclusion

A novel finite element framework able to simulate the effects of cyclic loadings experienced by a stented artery during a cardiac cycle was presented. Both cardiac wall movement and pressure changes were included in the simulations, proving that cardiac wall displacement is a substantial factor during fatigue analysis within coronary arteries. Moreover, the negative effect of localised plaque calcifications was demonstrated in both the stress/strain and fatigue life analyses, thus mechanical corroboration to the empirical evidence that CSF might be correlated to the presence of plaque calcifications (Iwami et al., 1998; Nakazawa et al., 2009). Further analyses on the effects of different typologies of calcifications should be performed in order to make this conclusion more

general. In this light, more efforts should be devoted to a better modelling of the plaque geometry and all its heterogeneous components (calcifications, micro-calcifications, lipid pools, anisotropic behaviour, etc.).

Future efforts will be devoted to this direction, together with the use of patient-specific images, that allow the creation of models incorporating a more realistic plaque geometry, as recently showed by means of OCT (Celi et al., 2013). In addition, other factors clinically correlated to CSF such as overlapping stents, curvature or stent length will be investigated.

Finally, it is worth noting that current standard guidelines for non-clinical engineering tests from FDA (FDA, 2010) do not yet require the inclusion of the vessel and plaque presence in the device performance analysis. The results from the present study provide convincing evidence that not only the inclusion of a stenotic, calcified vessel should be considered but, concerning epicardial coronary vessels, the peculiar surrounding environment represented by the cardiac wall displacement should be included in such finite element analyses.

Conflict of interest statement

None.

Acknowledgements

The authors would like to acknowledge the many valuable suggestions made by Peter Forbes, Royal Literary Fund Writer Fellow and Dr. Claudio Capelli from the Centre for Cardiovascular Imaging, UCL Institute of Cardiovascular Science & Cardiorespiratory Unit, Great Ormond Street Hospital for Children, NHS Trust, London, UK.

References

- Adlakha, S., Sheikh, M., Wu, J., Burket, M.W., Pandya, U., Colyer, W., Eltahawy, E., Cooper, C.J., 2010. Stent fracture in the coronary and peripheral arteries. *J. Interv. Cardiol.* 23, 411–419.
- Aoki, J., Nakazawa, G., Tanabe, K., et al., 2007. Incidence and clinical impact of coronary stent fracture after sirolimus-eluting stent implantation. *Catheter. Cardiovasc. Interv.* 69, 380–386.
- Argente dos Santos, H.A., Auricchio, F., Conti, M., 2012. Fatigue life assessment of cardiovascular balloon-expandable stents: a two-scale plasticity-damage model approach. *J. Mech. Behav. Biomed. Mater.* 15, 78–92.
- Bouma, B.E., Tearney, G.J., Yabushita, H., Shishkov, M., Kauffman, C.R., DeJoseph Gauthier, D., MacNeill, B.D., Houser, S.L., Aretz, H.T., Halpern, E.F., Jang, I.-K., 2003. Evaluation of intracoronary stenting by intravascular optical coherence tomography. *Heart* 89 (3), 317–320.
- Celi, S., Vagheti, M., Palmieri, C., Berti, S., 2013. Superficial coronary calcium analysis by OCT: looking forward an imaging algorithm for an automatic 3D quantification. *Int. J. Cardiol.* 168 (3), 2958–2960.
- Ding, Z., Friedman, M.H., 2000. Quantification of 3-D coronary arterial motion using clinical biplane cineangiograms. *Int. J. Cardiovasc. Imaging* 16, 331–346.
- Ebenstein, D.M., Coughlin, D., Chapman, J., Li, C., Pruitt, L.A., 2009. Nanomechanical properties of calcification, fibrous tissue, and hematoma from atherosclerotic plaques. *J. Biomed. Mater. Res. A* 91, 1028–1037.
- Food and Drug Administration Center for Devices and Radiological Health, 2010. Guidance for Industry and FDA Staff Non-clinical Engineering Tests and Recommended Labeling for Intravascular Stents and Associated Delivery Systems. Document issued on April 18, 2010.
- Gastaldi, D., Morlacchi, S., Nichetti, R., Capelli, C., Dubini, G., Petrini, L., Migliavacca, F., 2010. Modelling of the provisional side-branch stenting approach for the treatment of atherosclerotic coronary bifurcations: effects of stent positioning. *Biomech. Model. Mechanobiol.* 9, 551–561.
- Gervaso, F., Capelli, C., Petrini, L., Lattanzio, S., Di Virgilio, L., Migliavacca, F., 2008. On the effects of different strategies in modelling balloon-expandable stenting by means of finite element method. *J. Biomech.* 41, 1206–1212.
- Gijzen, F.G.H., Migliavacca, F., Schievano, S., Socci, L., Petrini, L., Thury, A., Wentzel, J.J., van der Steen, A., Serruys, P., Dubini, G., 2008. Simulation of stent deployment in a realistic human coronary artery. *BioMed. Eng. OnLine* 7, 23, <http://dx.doi.org/10.1186/1475-925X-7-23>.
- Grossman, W., Jones, D., McLaurin, L.P., 1975. Wall stress and patterns of hypertrophy in the human left ventricle. *J. Clin. Invest.* 56, 56–64.

- Halwani, D., Anderson, P., Brott, B., Anayiotos, A., Lemons, J., 2012. The role of vascular calcification in inducing fatigue and fracture of coronary stents. *J. Biomed. Mater. Res. Part B* 2012 (100B), 292–304.
- Hjortnaes, J., New, S.E., Aikawa, E., 2013. Visualizing novel concepts of cardiovascular calcification. *Trends Cardiovasc. Med.* 23, 71–79.
- Holzapfel, G.A., Sommer, G., Gasser, C.T., Regitnig, P., 2005. Determination of layer-specific mechanical properties of human coronary arteries with nonatherosclerotic intimal thickening and related constitutive modeling. *Am. J. Physiol. Heart Circ. Physiol.* 289, H2048–H2058.
- Hsiao, H.M., Chiu, Y.H., Lee, K.H., Lin, C.H., 2012. Computational modeling of effects of intravascular stent design on key mechanical and hemodynamic behaviour. *Comput.-Aided Design* 44, 757–765.
- Hsiao, H.M., Chiu, Y.H., Wu, T.Y., Shen, J.K., Lee, T.Y., 2013. Effects of through-hole drug reservoirs on key clinical attributes for drug-eluting depot stent. *Med. Eng. Phys.* 35, 884–897.
- Iwami, T., Fujii, T., Miura, T., Otani, N., Iida, H., Kawamura, A., Yoshitake, S., Kohno, M., Hisamatsu, Y., Iwamoto, H., Matsuzaki, M., 1998. Importance of left anterior descending coronary artery curvature in determining cross-sectional plaque distribution assessed by intravascular ultrasound. *Am. J. Cardiol.* 82, 381–384.
- Johnson, R.C., Leopold, J.A., Loscalzo, J., 2006. Vascular calcification: pathobiological mechanisms and clinical implications. *Circ. Res.* 99, 1044–1059.
- Kuramitsu, S., Iwabuchi, M., Haraguchi, T., Domei, T., Nagae, A., Hyodo, M., Yamaji, K., Soga, Y., Arita, T., Shirai, S., Kondo, K., Ando, K., Sakai, K., Goya, M., Takabatake, Y., Sonoda, S., Yokoi, H., Toyota, F., Nosaka, H., Nobuyoshi, M., 2012. Incidence and clinical impact of stent fracture after everolimus-eluting stent implantation. *Circ. Cardiovasc. Interv.* 5, 663–671.
- Li, J., Luo, Q., Xie, Z., Li, Y., Zeng, Y., 2010. Fatigue life analysis and experimental verification of coronary stent. *Heart Vessel.* 25, 333–337.
- Liao, R., Chen, S.Y.J., Messenger, J.C., Groves, B.M., Burchenal, J.E.B., Carroll, J.D., 2002. Four-dimensional analysis of cyclic changes in coronary artery shape. *Catheter. Cardiovasc. Interv.* 55, 344–354.
- Lim, H.B., Hur, G., Kim, S.Y., Kim, Y.H., Kwon, S.U., Lee, W.R., Cha, S.J., 2008. Coronary stent fracture: detection with 64-section multidetector CT angiography in patients and in vitro. *Radiology* 249, 810–819.
- Loree, H.M., Grodzinsky, A.J., Park, S.Y., Gibson, L.J., Lee, R.T., 1994. Static circumferential tangential modulus of human atherosclerotic tissue. *J. Biomech.* 27, 195–204.
- Marrey, R.V., Burgermeister, R., Grishaber, R.B., Ritchie, R.O., 2006. Fatigue and life prediction for cobalt-chromium stents: a fracture mechanics analysis. *Biomaterials* 27, 1988–2000.
- Martin, D., Boyle, F.J., 2011. Computational structural modelling of coronary stent deployment: a review. *Comput. Methods Biomech. Biomed. Eng.* 14 (4), 331–348.
- Morlacchi, S., Migliavacca, F., 2013. Modeling stented coronary arteries: where we are, where to go. *Ann. Biomed. Eng.* 41, 1428–1444.
- Morlacchi, S., Colleoni, S.G., Cárdenes, R., Chiastra, C., Diez, J.L., Larrabide, I., Migliavacca, F., 2013. Patient-specific simulations of stenting procedures in coronary bifurcations: two clinical cases. *Med. Eng. Phys.* 35, 1272–1281.
- Nakazawa, G., Finn, A.V., Vorpahl, M., Ladich, E., Kutys, R., Balazs, I., Kolodgie, F.D., Virmani, R., 2009. Incidence and predictors of drug-eluting stent fracture in human coronary artery a pathologic analysis. *J. Am. Coll. Cardiol.* 54, 1924–1931.
- Poncin, P., Proft, J., 2003. Stent tubing: understanding the desired attributes. In: *Proceedings of the Materials & Processes for Medical Devices Conference*.
- Prosi, M., Perktold, K., Ding, Z., Friedman, M.H., 2004. Influence of curvature dynamics on pulsatile coronary artery flow in a realistic bifurcation model. *J. Biomech.* 37, 1767–1775.
- Schievano, S., Taylor, A.M., Capelli, C., Lurz, P., Nordmeyer, J., Migliavacca, F., Bonhoeffer, P., 2010. Patient specific finite element analysis results in more accurate prediction of stent fractures: application to percutaneous pulmonary valve implantation. *J. Biomech.* 43, 687–693.
- Shaikh, F., Maddikunta, R., Djelmami-Hani, M., Solis, J., Allaqaband, S., Bajwa, T., 2008. Stent fracture, an incidental finding or a significant marker of clinical in-stent restenosis? *Catheter. Cardiovasc. Interv.* 71, 614–618.